Geotextiles and Geomembranes 35 (2012) 14–24

Contents lists available at SciVerse ScienceDirect

Geotextiles and Geomembranes

journal homepage: www.elsevier.com/locate/geotexmem

Performance of geocell-reinforced recycled asphalt pavement (RAP) bases over weak subgrade under cyclic plate loading

Jitendra K. Thakur [a], Jie Han [a,*], Sanat K. Pokharel [b], Robert L. Parsons [a]

[a] Department of Civil, Environmental, & Architectural Engineering, University of Kansas, 2150 Learned Hall, 1530 West 15th Street, Lawrence, KS 66045, USA
[b] Paradox Access Solutions Inc., St. Albert, AB, T8N 7L5 Canada

ARTICLE INFO

Article history:
Received 4 December 2011
Received in revised form
28 May 2012
Accepted 21 June 2012
Available online 24 July 2012

Keywords:
Geocell
RAP
Permanent deformation
Vertical stress
Strain
Improvement factor

ABSTRACT

Recycled Asphalt Pavement (RAP) is the most reused and recycled material in the United States. It has been included at percentage of 15–50% in new hot mix asphalt (HMA) concrete and used as a base course material up to 100% for pavement construction. Due to the existence of asphalt in RAP, RAP base courses may have increased or excessive permanent deformation under traffic loading. To minimize such deformation, use of geocell was proposed by authors to confine RAP. To verify the performance of geocell-reinforced RAP bases and the benefit of geocell reinforcement, an experimental study was conducted on geocell-reinforced RAP bases over a weak subgrade under cyclic plate loading. A large geotechnical test box was used for the cyclic plate loading tests. The subgrade was a mixture of sand and kaolin and compacted at the moisture content corresponding to a California Bearing Ratio (CBR) value of 2%. The fractionated RAP was compacted at the moisture content close to the optimum value. A total of four sections with three base thicknesses (0.15, 0.23, and 0.30 m) were prepared and tested, which included one 0.30 m thick unreinforced section and three geocell-reinforced sections. During the testing, surface deformations and vertical stresses at the interface of base and subgrade and strains in geocell walls were monitored. Test results show that the geocell-reinforced RAP bases had much smaller permanent deformations than the unreinforced RAP bases. The geocell-reinforced bases reduced the vertical stresses at the interface between base and subgrade as compared with the unreinforced base. The strain measurements demonstrated that the thicker geocell-reinforced RAP base behaved as a slab while the thinner base behaved as a tensioned membrane. The experimental results indicated that novel polymeric alloy (NPA) geocell reinforcement improved the life of 0.15, 0.23, and 0.30 m thick reinforced RAP base sections by factors of 6.4, 3.6, and 19.4 at a permanent deformation of 75 mm as compared with the 0.30 m thick unreinforced section at the same permanent deformation, respectively. Geocell reinforcement increased the minimum stress distribution angle by 2°, 3.5°, and 7° for the 0.15, 0.23, and 0.30 m thick reinforced RAP base sections as compared with the unreinforced section.

1. Introduction

Recycled Asphalt Pavement (RAP) is a removed and reprocessed pavement material containing asphalt binder and aggregates. RAP is obtained either by milling or by a full depth recovery method. Literature review shows that RAP has been mostly used with new asphalt binder to form hot-mix asphalt (HMA) concrete as a pavement layer. The percentage of RAP used in the HMA concrete typically ranges from 15% to 50%. RAP has also been used as a granular base material in paved and unpaved roadways, parking areas, bicycle paths, gravel road rehabilitation, shoulders, residential driveways, trench backfill, engineered fill, and culvert backfill (User Guidelines for Byproducts and Secondary Use Materials in Pavement Construction, 2008).

California, Colorado, Montana, and New Jersey DOTs have used RAP as a base course material (McGarrah, 2007). Past research showed that 100% RAP does not produce a product of base course quality as the CBR value and shear strength of RAP decrease with increasing percentage of RAP (McGarrah, 2007). It was reported that the CBR value for 100% RAP was 11%, but when the RAP percentage decreased to 80% after being mixed with virgin aggregate, the CBR value increased to 26% (Taha et al., 1999). However, Locander (2009) found that RAP had similar engineering pavement design properties as unbound aggregate. Canadian Strategic Highway Research Program (2000) concluded that the permanent deformation of RAP bases depends on magnitude, frequency,

* Corresponding author. Tel.: +1 785 864 3714; fax: +1 785 864 5631.
E-mail address: jiehan@ku.edu (J. Han).

0266-1144/$ – see front matter © 2012 Elsevier Ltd. All rights reserved.
http://dx.doi.org/10.1016/j.geotexmem.2012.06.004

pressure, and speed of loading; temperature; aggregate gradation, shape and texture; binder type and amount; and construction variables such as compaction, quality control, and segregation. Bennert and Maher (2005) found that permanent deformation of the RAP-aggregate blend increased with the percentage of RAP using cyclic triaxial tests. It was also confirmed that the permanent deformation was a function of the shape of aggregate particles in RAP and depended on the gradation of the aggregates (Bennert and Maher, 2005). The authors believe that instead of blending RAP with virgin aggregate, geosynthetics may be used to reinforce a RAP base course to increase its strength and stiffness.

Geosynthetics have been widely used as construction materials for soil reinforcement in civil engineering projects such as slopes, retaining walls, roads, landfills, foundations, etc. since 1970s. Geosynthetic reinforcement has been one of the established techniques for subgrade improvement and base reinforcement for over 40 years (Giroud and Han, 2004a, b). Today, there are many types of geosynthetic products (e.g., geogrid, geotextile, geocell, geomembrane, etc.) available in the market. Each product is designed to solve a specific type of civil engineering problems. Geocell is a three-dimensional interconnected honeycomb type of geosynthetics used to confine unbound aggregates for base courses in roads since 1970s. Rajagopal et al. (1999) investigated the influence of geocell confinement on the strength and stiffness behavior of granular soil confined in single and multiple geocells and found that the apparent cohesive strength of granular soil increased due to geocell confinement. They also found that the induced apparent cohesive strength depended on the tensile modulus of geocell, however geocell confinement had no effect on frictional strength of granular soil. A comprehensive literature review by Yuu et al. (2008) indicated that theories and design methods for geocell were far behind its applications in the field up to that time, especially for roadway applications because the mechanisms of geocell reinforcement were not well understood and there was not enough research data.

Since then, Boushehrian et al. (2011), Han et al. (2008, 2011), Latha and Murthy (2007), Pokharel et al. (2010, 2011), Moghaddas Tafreshi and Dawson (2010a,b, 2012), Yang et al. (2012), and Zhang et al. (2009) have made significant efforts to improve the understanding of the mechanisms of geocell confinement and verify the performance of geocell-reinforced granular materials. A preliminary study done by Thakur et al. (2011) indicated the benefit of geocell in minimizing the creep deformation of RAP bases. Boushehrian et al. (2011) investigated the cyclic behavior of reinforced sand by conducting a series of laboratory tests, field tests, and numerical modeling using PLAXIS 3D Tunnel software and reported the benefit of the three-dimensional reinforced system (a grid-anchor reinforcement system) over the conventional geomesh system in reducing the settlements of foundations rested on sand bed. Latha and Murthy (2007) conducted triaxial tests to study the effect of planar, cellular, and discrete fiber reinforcements on strength improvement of geosynthetic-reinforced sand through regular triaxial compression tests. Cellular reinforcement was found to be more effective in improving the strength compared to planar and discrete reinforcements. Moghaddas Tafreshi and Dawson (2010a,b; 2012) showed the benefits of 3D geosynthetics (geocell or 3D reinforcement system made with geotextile) over planar geosynthetics (geotexile) in improving bearing capacity and reducing settlements of strip footings on sand by conducting a series of small-scale laboratory model tests on 3D geosynthetic-reinforced (geocell or 3D geotextile), geotextile-reinforced, and unreinforced sand. Zhang et al. (2009) developed a theoretical solution for the deformation of a geocell-reinforced soil layer as a beam on Winkler's foundation. Han et al. (2011), Pokharel et al. (2011), and Yang et al. (2012) reported the accelerated pavement testing of geocell-reinforced unpaved roads with different infill materials (sand, quarry waste, well-graded aggregate, and RAP). They demonstrated the benefits of geocell in reducing permanent deformations and increasing stress distribution angles; however, accelerated pavement testing is costly and the facility is not readily available for most research institutes. Large-scale box test results were used by Giroud and Han (2004a, b) to calibrate the design method for geosynthetic-reinforced unpaved roads. A preliminary study done by Thakur et al. (2012) investigated the benefit of geocell reinforcement on two 0.3 m thick RAP base sections (unreinforced and reinforced) over weak subgrade. This paper reports four large-scale box tests to evaluate the performance of geocell-reinforced RAP bases over weak subgrade under cyclic loading.

In this study, geocell was proposed to minimize the permanent deformations of RAP bases and improve their performance under cyclic loading through confinement. Four laboratory cyclic plate load tests were conducted in a large geotechnical test box at the University of Kansas to investigate the benefits of geocell on the reduction in the permanent deformations and the vertical stresses at the interface between base and subgrade as compared with an unreinforced base.

2. Test materials and equipments

2.1. Geocell

The geocell, made of novel polymeric alloy (NPA), was manufactured and provided by PRS Mediterranean, Ltd. in Israel. It has three-dimensional honeycomb-interconnected cells as shown in Fig. 1. The geocell used in this study had two perforations of 100 mm^2 area each on each pallet, 1.1-mm wall thickness, 100 and 150 mm cell heights, 19.1-MPa tensile strength, and 355-MPa elastic modulus at 2% strain. The tensile strength and elastic modulus were determined based on the tensile tests of geocell sheets at a strain rate of 10%/min at 23 °C. Other material properties of NPA geocell are shown in Table 1, and are the same as those reported in Yang et al. (2012). The NPA is characterized by flexibility at low temperatures similar to HDPE with elastic behavior similar to engineering thermoplastic.

2.2. Geotextile

A 3.5 oz (99.65 g) non-woven geotextile was placed at the interface of subgrade and base course as a separator in all the

Fig. 1. Geocell infilled with RAP.

Table 1
Material properties of the NPA geocell (provided by the manufacturer).

Properties		Description	Unit	Test method
Tensile strength		>20	N/mm	PRS method
Tensile modulus at 1% strain		462	N/mm	
Allowed strength for design of 50 years		>5.7	N/mm	ASTM D 6992
Creep reduction factor		<3.5		ASTM D 6992
Coefficient of thermal expansion (CTE)		≤80	ppm/°C	ISO 11359-2 ASTM E 831
Flexural storage modulus at	30 °C	>750	MPa	ISO 6721-1
	45 °C	>650		ASTM E 2254
	60 °C	>550		
	80 °C	>300		
Oxidative induction time (OIT)		≥100	min	ISO 11375-6 ASTM D 3895 (OIT @ 200 °C, 25 kPa)
Durability of UV degradation		≥400	min	ASTM D 5885 (HPOIT @ 150 °C, 3500 kPa)

reinforced test sections over weak subgrade in the large geotechnical test box. The material properties of geotextile are shown in Table 2, and are same as those provided in Yang et al. (2012).

2.3. Base course

Recycled asphalt pavement (RAP) milled from a city street in Lawrence, Kansas was used as the base material in this study. It was a fractionated RAP material (sometimes named as FRAP) and provided by R.D. Johnson Excavating, Co., Lawrence, Kansas. The properties of the RAP material were determined by laboratory tests following different ASTM standards and are presented in Table 3. The fine and coarse aggregates were extracted from RAP by an ignition method whereas asphalt was extracted by a centrifuge method for determining its properties. Fig. 2 shows the gradation curves of the RAP aggregates extracted by the ignition method before and after compaction. There were minor changes in the gradation curves after compaction.

Five modified Proctor compaction tests were performed on RAP specimens at different moisture contents following ASTM D 1557 to obtain the compaction curve as shown in Fig. 3.The maximum dry density was about 1.96 g/cm^3, which corresponds to the optimum moisture content (OMC) of 6.6%. Also, five unsoaked California Bearing Ratio (CBR) tests were performed on laboratory-compacted RAP specimens at different moisture contents following ASTM D 1188 to obtain the CBR versus moisture content curve as shown in Fig. 3. As discussed later, the average CBR value of the RAP base over the subgrade in each test was approximately 11% when compacted at 5.5% moisture content inside the large-scale test box. This CBR value was estimated by the Dynamic Cone Penetration (DCP) test conducted after preparation of the base over subgrade using Eq. (1) (Webster et al., 1994). The lower CBR value of the base material in the box test than that in the laboratory compaction mold might result from less confinement and lower energy of compaction of the base course in the large-scale test box.

Table 2
Material properties of the geotextile (provided by the manufacturer).

Properties	Description	Unit	Test method
Grab tensile strength	0.401	kN	ASTM D 4632
Grab elongation	50	%	ASTM D 4632
Trapezoid tear strength	0.178	kN	ASTM D 4533
Puncture resistance	0.267	kN	ASTM D 4833
Mullen burst strength	1378	kPa	ASTM D 3786
Permittivity	2.2	1/s	ASTM D 4491
Water flow	6095	1/min/m^2	ASTM D 4491
Apparent opening size (AOS)	0.212	mm	ASTM D 4751

$$\mathrm{CBR} = \frac{292}{(\mathrm{PI})^{1.12}} \tag{1}$$

where PI = Penetration Index (mm/blow), which is calculated based on the amount of penetration per each blow.

2.4. Subgrade

Subgrade was prepared artificially by mixing 25% Kaolin and 75% Kansas River (KR) sand. The KR sand used in this study was a poorly-graded sub-rounded river sand whose properties are shown in Table 3. The plastic and liquid limits of the subgrade soil were found to be 22% and 30%, respectively, following the test standard ASTM D4318-10. Six standard Proctor compaction tests were performed at different moisture contents to obtain the compaction curve for this subgrade as shown in Fig. 3b. The maximum dry density of this mix was about 2.01 g/cm^3, which corresponds to the optimum moisture content of 10.8%. Six laboratory unsoaked CBR tests were performed on laboratory compacted subgrade at different moisture contents to obtain the CBR versus moisture content curve as shown in Fig. 3b. The subgrade soil was compacted at 11.4% moisture content in the large box tests to achieve a target CBR value of approximately 2%, which was verified by vane shear tests during the subgrade preparation and DCP tests after the test section preparation. Holtz et al. (2008) suggested that the optimum use of geosynthetics in roadway construction is when the CBR of the subgrade soil is less than 3%. Therefore, the subgrade CBR of 2% was chosen to evaluate the benefit of geocell reinforcement to improve the performance of bases over weak subgrade. The CBR values were estimated by vane shear tests using Eq. (2) specially developed for this subgrade (Pokharel, 2010).

$$\mathrm{CBR} = \frac{C_u}{20.5} \tag{2}$$

where C_u = vane shear strength of subgrade (kPa).

2.5. Test setup

Four cyclic plate load tests were conducted in a large geotechnical testing box (2.2 m × 2.0 m × 2.0 m high) to evaluate the performance of RAP reinforced by geocell over weak subgrade as shown in Fig. 4. The four test sections were 0.30 m thick unreinforced, 0.15 m thick reinforced, 0.23 m thick reinforced, and 0.30 m thick reinforced base courses over weak subgrade. Each test section included 1.0 m thick subgrade soil prepared at 11.4% moisture content, which corresponds to 2% CBR. For the 0.30 m thick unreinforced RAP base, RAP was placed on the top of the subgrade and compacted by a vibratory plate compactor in three lifts (0.1 m each). A layer of geotextile was placed on the top of the subgrade in the three reinforced sections. For the 0.15 m and 0.23 m thick reinforced RAP base courses, 100 mm and 150 mm high geocells were installed on the top of the geotextile, respectively and then were filled with RAP and compacted by hand tamping inside each cell. A RAP cover of about 50 mm or 80 mm thick was added on the filled geocell for the 0.15 m or 0.23 m thick section for the protection of geocells. The cover material was compacted by the vibratory plate compactor. Similarly, the 0.30 m thick reinforced section was prepared in four lifts (i.e. the first 100 mm high geocell plus 30 mm thick cover and the second 100 mm high geocell plus 70 mm thick cover). For each test section, the RAP material of every

Table 3
Properties of the RAP and subgrade materials used in this study.

	Aggregate			Test method
RAP material	Bulk specific gravity	Fine aggregate	2.48	ASTM C 128
		Coarse aggregate	2.39	ASTM C 127
	SSD bulk specific gravity	Fine aggregate	2.56	ASTM C 128
		Coarse aggregate	2.49	ASTM C 127
	Uncompacted void content	Fine aggregate	39.15%	ASTM C 1252 (Method B)
	Mean particle size (d_{50}) (mm)		2.0	
	Coefficient of curvature (C_c)		0.85	
	Coefficient of uniformity (C_u)		8.33	
	Asphalt binder			
	Binder content	Centrifuge method	6.71%	ASTM D 2172
		Ignition method	6.87%	ASTM D 6307
	Viscosity of asphalt binder at 135 °C (Pa-s)		1.408	ASTM D 1856
Kansas River (KR) sand used in subgrade mix	Specific gravity		2.62	ASTM C 128
	Mean particle size (d_{50}) (mm)		0.54	
	Coefficient of curvature (C_c)		0.95	
	Coefficient of uniformity (C_u)		3.1	

lift was compacted to a target density corresponding to 95% of the maximum dry density on the drier side of compaction curve within 2% range of moisture content. The quantities (weights) of subgrade and RAP material for each lift of compaction were calculated by multiplying the density of the material by the soil volume to fill. The instrumentation and data acquisition system included earth pressure cells, displacement transducers, and strain gages and the locations of these sensors are shown in Fig. 4. The pressure cells used in the tests were strain gage type, and were made of stainless steel, had a thickness of 11.3 mm, an outer diameter of 50 mm with the sensing area diameter of 46 mm, and total weight of 160 g. It had minute displacement of pressure-sensitive area due to double diaphragm structure and non linearity of 1% RO (random occurrence). The accuracies of earth pressure cells, displacement transducers, and strain gages were 0.001 kPa, 0.01 mm, and 10^{-6}, respectively.

The servo hydraulic MTS loading system consisted of a loading frame, a hydraulic actuator, and a servo-control unit connected to both a data acquisition system and a hydraulic control valve. The steel loading plate had a diameter of 300 mm and a thickness of 30 mm. An additional 10 mm thick rubber base was attached at the bottom of the loading plate to simulate rubber tire contact. The cyclic load was applied with a peak force of 40 kN and a trough force of 0.5 kN at a wave frequency of 0.77 Hz as shown in Fig. 5. The box, the loading plate, and the loading type were the same as those used by Qian et al. (2011). Qian et al. (2011) verified the repeatability of the test method and results. The peak load was selected to simulate a single wheel load of 40 kN (equal to an axle load of 80 kN and a tire contact pressure of 550 kPa). The wave frequency of 0.77 Hz was chosen based on previous studies to simulate field traffic speed.

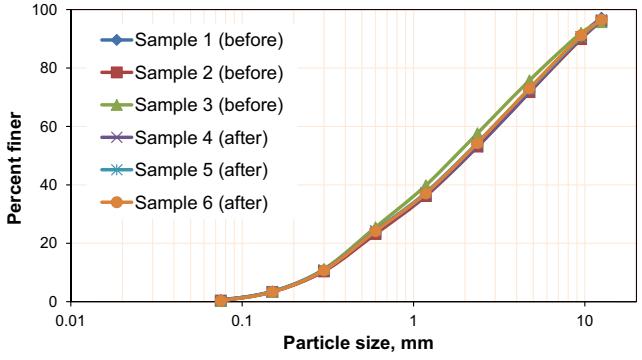

Fig. 2. Gradation curves of the RAP aggregates extracted by the ignition method before and after compaction.

3. Results and discussion

3.1. Vane shear, DCP, and sand cone test results

Vane shear tests were performed just after the preparation of the subgrade for each test to confirm that the target CBR was achieved.

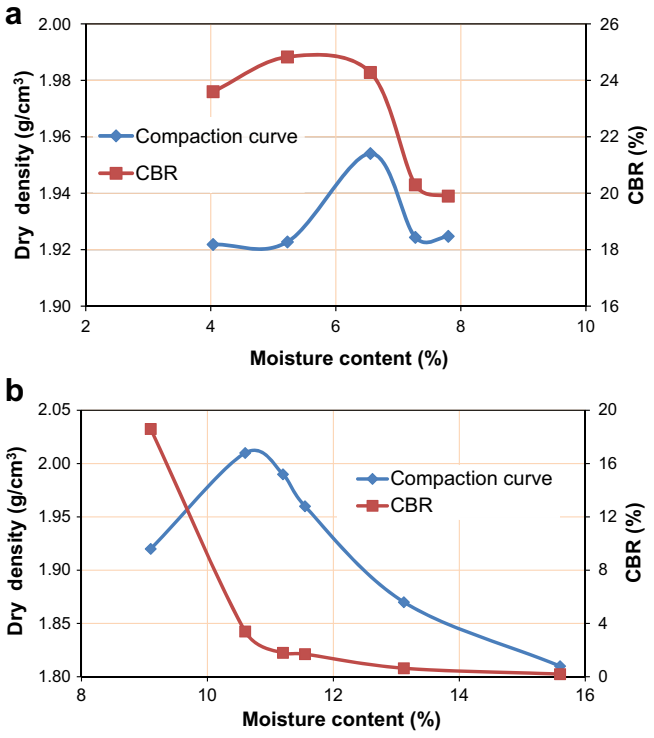

Fig. 3. Compaction and CBR curves. (a) RAP (Thakur et al., 2012), (b) Subgrade.

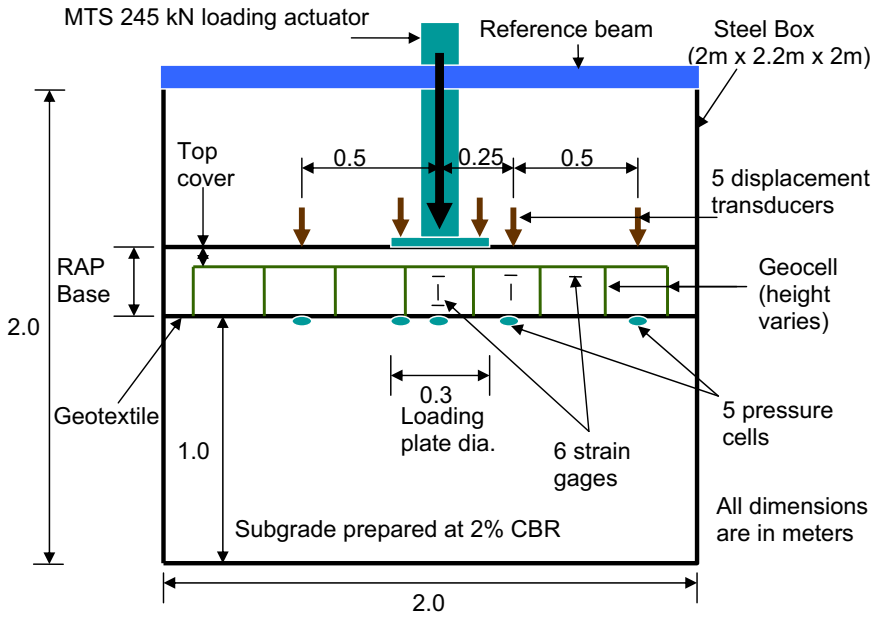

Fig. 4. Cross-section of the test section and locations of sensors (Thakur et al., 2012).

After each cyclic plate load test, two sand cone tests in accordance with ASTM D15556-07 were conducted to evaluate the density of the compacted RAP base. Vane shear, DCP, and sand cone test results for geocell-reinforced and unreinforced test sections are presented in Table 4.

The slightly higher subgrade CBR values were obtained during DCP tests because the DCP tests were conducted one day after the preparation of the test sections and some compaction energy also went to the subgrade during base material compaction. The base course in the 0.23 m reinforced section was less compacted as compared with the base courses in the unreinforced and other reinforced sections based on these measurements. Less compaction of the 0.23 m thick reinforced section affected its performance as discussed later.

3.2. Permanent deformation

Vertical displacements on the surface were measured at five locations using displacement transducers as shown in Fig. 4. Fig. 6 presents the recorded displacements of the loading plate (averaged from two displacement transducers) developing with the number of loading cycles during all the tests, which included accumulated permanent (plastic) deformation and resilient deformation (elastic rebound). The permanent deformation of the loading plate at least 75 mm was used as the criterion to terminate each cyclic loading test. This criterion was used by Hammitt (1974) and Giroud and Han (2004a, b) to define the failure of unpaved roads. However, the test for the 0.30 m thick reinforced section stopped after 45 cycles and 59.1 mm permanent deformation due to malfunction of the controller. The average permanent deformations of the unreinforced and reinforced base courses at the center versus the number of loading cycles are shown in Fig. 7. The test data for the 0.30 m thick reinforced section were extrapolated up to 75 mm deformation for comparative purposes and the extrapolated portion is presented by the dotted line. The trend of extrapolation was determined by plotting the test data in a semi-log scale (i.e. the permanent deformation in the linear scale and the number of loading cycles in the log10 scale). The plotted data showed a linear relationship in the semi-log graph after initial 17 cycles. It is shown that the permanent deformation increased with the number of loading cycles. The rate of the increase in the permanent deformation decreased with an increase of the loading cycles. The amount of permanent deformation increased rapidly during the first few loading cycles and then increased at a reduced rate for the reinforced bases. However, the permanent deformation increased sharply until failure for the unreinforced base. Therefore, the reinforced bases showed a stabilizing response with a reduced rate of plastic deformation and great resilience after the initial few cycles whereas the unreinforced base had a non-stabilizing response with an increased rate of plastic deformation and little resilience. Moghaddas Tafreshi and Dawson (2010b) obtained the similar results of permanent deformation versus number of loading cycles for the geocell-reinforced sand bed. At the maximum allowable deformation of 75 mm, the unreinforced (0.30 m thick) and reinforced (0.15, 0.23 and 0.30 m thick) bases lasted for 5, 32, 18, and 97 loading cycles respectively. In other words, the numbers of loading cycles at 75 mm permanent deformation for the 0.15, 0.23, and 0.30 m thick reinforced RAP base sections were 6.4, 3.6, and 19.4 times that for the 0.30 m thick unreinforced RAP base section, respectively. Due to the low loading cycles for the 0.30 m thick unreinforced section, unreinforced sections with thinner bases (0.15 and 0.23 m thick) were not tested. Fig. 7 shows that the 0.23 m thick reinforced base lasted for fewer loading cycles than the 0.15 m thick reinforced base. This result was due to less compaction resulting in a lower CBR value of the base in the 0.23 m thick base

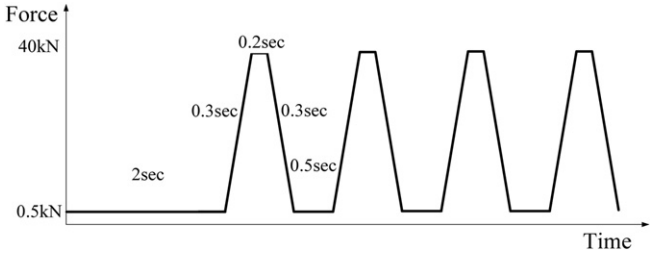

Fig. 5. Cyclic loading curve.

Table 4
Vane shear, DCP, and sand cone test results.

Test sections	Subgrade		Base course		
	Average CBR, % (vane shear)	Average CBR, % (DCP)	Average CBR for RAP inside geocell pocket (DCP)	Average CBR of whole RAP base, % (DCP)	Relative compaction, % (sand cone)
0.15 m reinforced	2.1	2.8	10.8	11.4	93
0.23 m reinforced	1.9	2.0	6.1	6.3	84
0.30 m reinforced	2.0	2.1	9.6	10.2	91
0.30 m unreinforced	1.9	2.0	N/A	10.2	91

Note: N/A indicates that CBR for RAP inside geocell's pocket for 0.30 m unreinforced section is not available.

section compared to that in the 0.15 m thick base section. Among all the test sections, the unreinforced RAP base section had the largest permanent deformation while the 0.30 m thick reinforced base section had the smallest permanent deformation. The 0.23 m and 0.15 m thick reinforced base sections had smaller permanent deformation than the 0.30 m thick unreinforced section. These comparisons clearly demonstrate the benefit of geocell in improving the performance of the RAP base over the unreinforced section. The test results also suggested that the compaction of RAP in the geocell-reinforced base played an important role in the performance of the test section.

Fig. 8 presents the distributions of surface permanent deformations at the center, 250 mm, 500 mm, and 750 mm away from the center of the loading plate at the 5th loading cycle for each test. Since the 0.30 m thick unreinforced section failed only after 5 cycles, the loading cycles of 5 was chosen for the comparison purpose. Only a small amount of compression was observed at 250 mm away from the center for all test sections except the 0.23 m thick reinforced section. The 0.23 m reinforced section showed a small amount of heave at 250 mm away from the center. The unreinforced section showed more compression at the center and more heave at 500 mm and 750 mm away from the center than the reinforced sections.

3.3. *Resilient deformation*

The resilient deformation and percentage of resilient deformation at the center versus the number of loading cycles are presented in Figs. 9 and 10, respectively. The resilient deformation is defined as the rebound of the test section when unloaded from the maximum load (40 kN) to the minimum load (0.5 kN). The percentage of resilient deformation was calculated by dividing the resilient deformation at each load cycle to the total deformation (i.e., the sum of resilient and plastic deformations) at that cycle. The amount of resilient deformation and percentage of resilient deformation increased rapidly during the first few loading cycles but stabilized quickly to a constant value for the reinforced bases. However, the unreinforced base showed less sharp increase and a much curtailed response compared to the reinforced bases. The reinforced bases shook down to a steady state showing largely resilient behavior whereas the unreinforced base did not shake down to a steady state and underwent continuous plastic deformation without showing much resilience. The maximum resilient deformations for the reinforced and unreinforced bases were about 10 mm and 2.7 mm, respectively. The percentages of resilient deformation were 90.6%, 89.2%, 94.5%, and 13.3% for the 0.15, 0.23, 0.30 m thick reinforced and 0.30 m thick unreinforced base sections, respectively. The unreinforced RAP base section had the lowest percentage of resilient deformation among all the test sections while the 0.30 m thick reinforced base section had the highest percentage of resilient deformation at the end of tests. Overall, the resilient deformations and percentages of resilient deformations among all the reinforced sections were close. The exact reasons for their close resilient deformations and percentages of resilient deformation among three reinforced sections are unknown. The resilient and total deformations on the surface under each loading cycle depend on the deformations of the RAP base and the subgrade, and that induced by the slab or tensioned membrane effect of the geocell-reinforced base. Numerical analysis is needed to separate the contribution by each component, which will be performed in the future. The slab effect (also referred as a beam effect) is used to describe a structural element with bending resistance while the tensioned membrane effect is used to describe a structural element with tensile resistance but no bending resistance. These results demonstrate that the geocell improved the resilient behavior and reduced the plasticity of the test section after an initial period of plastic strain accumulation which might be associated with locking up of the geocell framework.

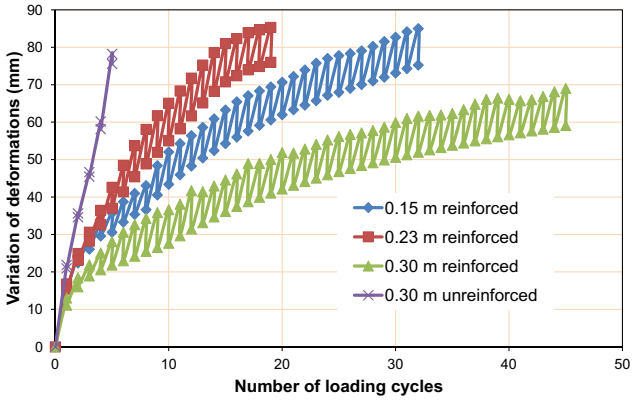

Fig. 6. Variation of deformations versus number of loading cycles.

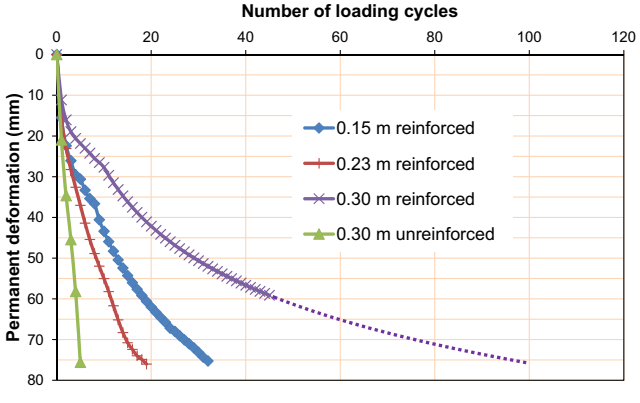

Fig. 7. Permanent deformation at the center of the plate versus the number of loading cycles.

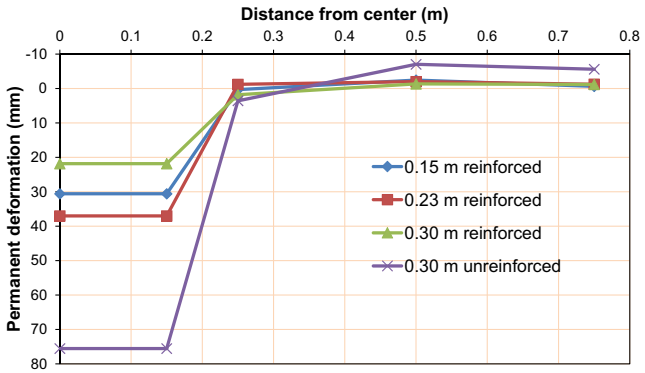

Fig. 8. Distributions of surface permanent deformations at different locations at the 5th loading cycle.

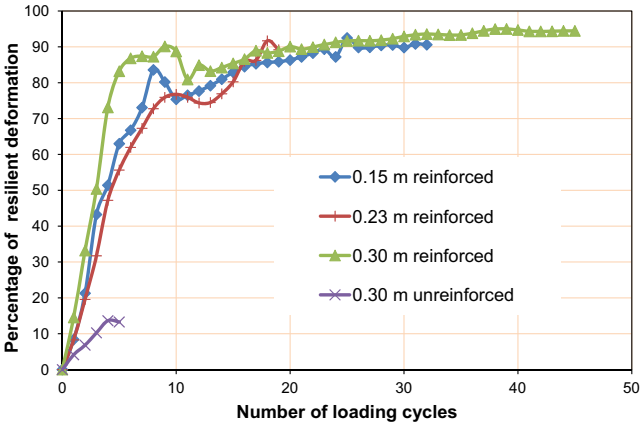

Fig. 10. Percentage of resilient deformation at the center versus the number of loading cycles.

3.4. Maximum vertical stress

The vertical stresses at the interface of subgrade and base course were measured by the earth pressure cells located at 0, 125, 250, 500, and 750 mm from the center of the loading plate. In the reinforced bases, no pressure cell was placed at the 750 mm location due to the shortage of the pressure cells during those tests. Fig. 11 shows the measured vertical stresses versus the number of loading cycles at the center and 125 mm away from the center. At these two locations, the maximum vertical stresses occurred. It is shown that the vertical stresses increased rapidly during the initial cycles and later they decreased slowly by a small magnitude or stabilized to a constant value for the reinforced cases. For the unreinforced case, the vertical stresses kept increasing until failure. The maximum vertical stresses measured at the center and 125 mm away from the center were 291 and 329 kPa; 159 and 210 kPa; 144 and 144 kPa; and 197 and 182 kPa for the 0.15, 0.23, 0.30 m thick reinforced and 0.30 m thick unreinforced base sections, respectively. The reduction of the vertical stresses in the reinforced sections resulted from the slab or tensioned membrane effect. The slab effect was observed for the thicker section whereas the tensioned membrane effect was observed for the thinner sections in the measurement of the strains on the geocell walls, which are presented and discussed later. Qian et al. (submitted for publication) found that the tensioned membrane effect became significant when the vertical permanent deformation reached 33% the base thickness. In this study, the reduction of the vertical stress happened at the permanent deformations of 48, 52, and 22 mm (i.e., the numbers of loading cycles of 12, 8, and 5) for the 0.15, 0.23, and 0.30 m thick reinforced sections, respectively, which correspond to 32%, 22%, and 7% their base thicknesses. These results imply that the 0.15 m thick reinforced base behaved as a tensioned membrane while the 0.30 m thick reinforced base behaved as a slab and the 0.23 m thick reinforced base behaved as a slab first and then a tensioned membrane. Therefore, the slab effect had a recognized benefit at a smaller permanent deformation than the tensioned membrane effect. The maximum vertical stress was highest in the 0.15 m thick reinforced base section and lowest in the 0.30 m thick reinforced base section. It is no surprise for the 0.15 m thick reinforced section to have higher vertical stresses at the interface than those in the 0.30 mm unreinforced section because of their large thickness difference. Even though the 0.15 m thick reinforced section had the higher vertical stresses, it lasted much

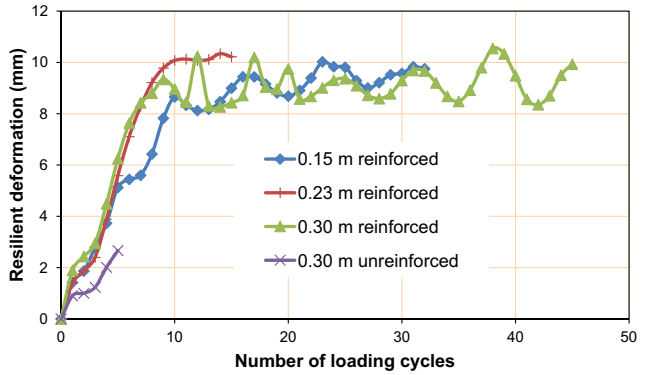

Fig. 9. Risilient deformation at the center versus the number of loading cycles.

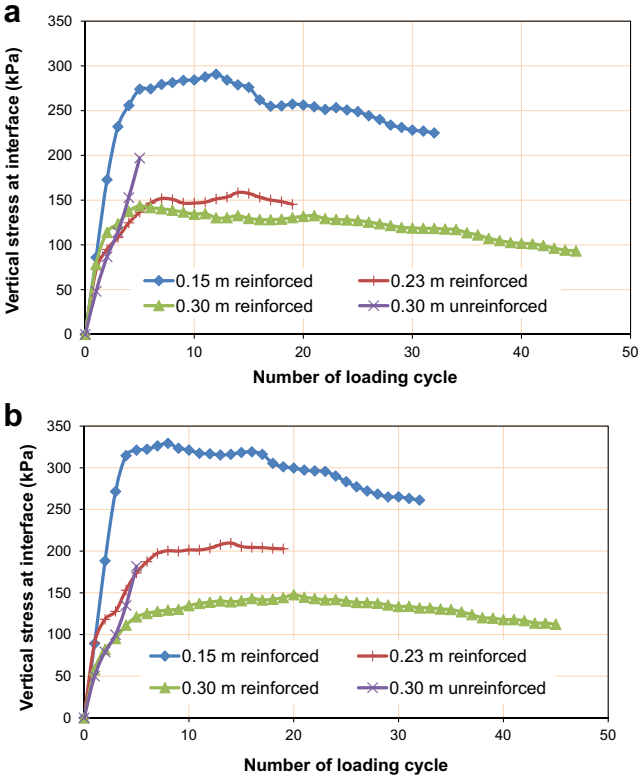

Fig. 11. Vertical stresses at the interface of subgrade and base. (a) At the center, (b) At 125 mm away from the center.

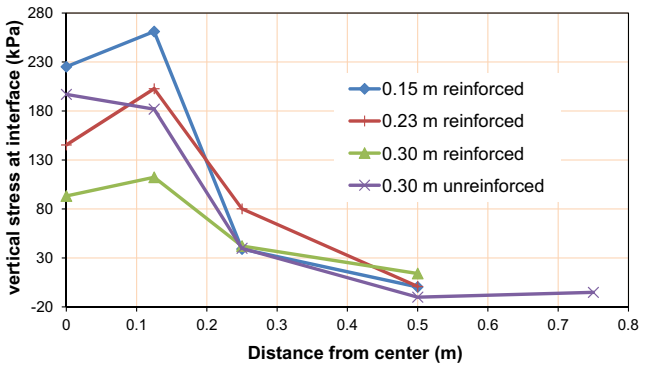

Fig. 12. Vertical stress distributions at the interface of subgrade and base at the end of test.

longer to reach the failure criterion of 75 mm than the 0.30 m thick unreinforced section. The increased road life demonstrates the effect and benefit of the geocell reinforcement. In addition, at the same base thickness, the 0.30 m thick reinforced section had much lower vertical stresses than the 0.30 m thick unreinforced section. These comparisons demonstrate that the vertical stresses at the interface decreased with an increase of base thickness and geocell reinforcement.

3.5. Vertical stress distribution

Fig. 12 presents the vertical stress distributions along the interface of subgrade and base at the end of the tests. The vertical stresses at 125 mm from the center were slightly higher than those at the center except for the unreinforced section. The vertical stresses for the unreinforced and reinforced bases decreased rapidly at the distances of more than 125 mm away from the center and the lowest vertical stresses were observed at the farthest distance from the center. The section having higher vertical stresses at the center and 125 mm away from the center showed lower vertical stresses at the remaining locations compared to other sections. This result follows the force equilibrium, i.e., the applied force is equal to the reaction force, which is equal to the total area under the stress distribution curve. The higher stresses at a distance of 125 mm away from the center in the thinner (0.15 and 0.23 m thick) sections might be caused by the vertical stress distribution underneath the rigid loading plate (i.e., the vertical stress near the edge is much higher than that in the center as shown by Muki (1961) in his theoretical solution).

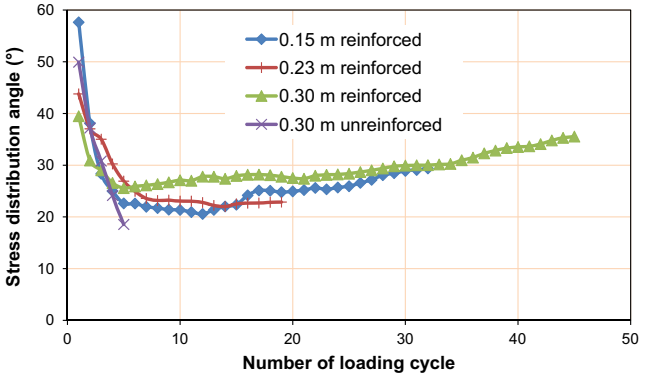

Fig. 13. Stress distribution angle versus the number of loading cycles.

The influence of this stress distribution became less significant when the depth increased. This is why such a distribution did not appear in the 0.30 m thick unreinforced and reinforced sections.

The vertical stress at the center of the interface can be approximately expressed in terms of a stress distribution angle as follows:

$$p_i = \frac{P}{\pi(r + h\tan\alpha)^2} \tag{3}$$

where p_i = the distributed vertical stress at the center of the interface of base course and subgrade (kPa); P = the applied load (i.e., 40 kN in this study); r = the radius of the plate contact area (i.e., 0.15 m); h = the thickness of the base course (m, varied); and α = the stress distribution angle in degree with respect to the vertical. The calculated stress distribution angles for four test sections at each loading cycle are shown in Fig. 13. The initial distribution angle depended on the initial conditions of the base and subgrade. It is shown that the stress distribution angle decreased rapidly within the first few loading cycles. The reduction in the stress distribution angle was attributed to the deterioration of the base quality (Giroud and Han, 2004a,b; Qian et al., 2011). The stress distribution angle approached a constant value or increased slowly for the reinforced sections, which demonstrated the stable response behavior. The increase of the stress distribution angle resulted from the slab effect and/or tensioned membrane effect by the geocell-reinforced layer, which is similar to a tensioned membrane effect by a planar reinforcement at large deformation.

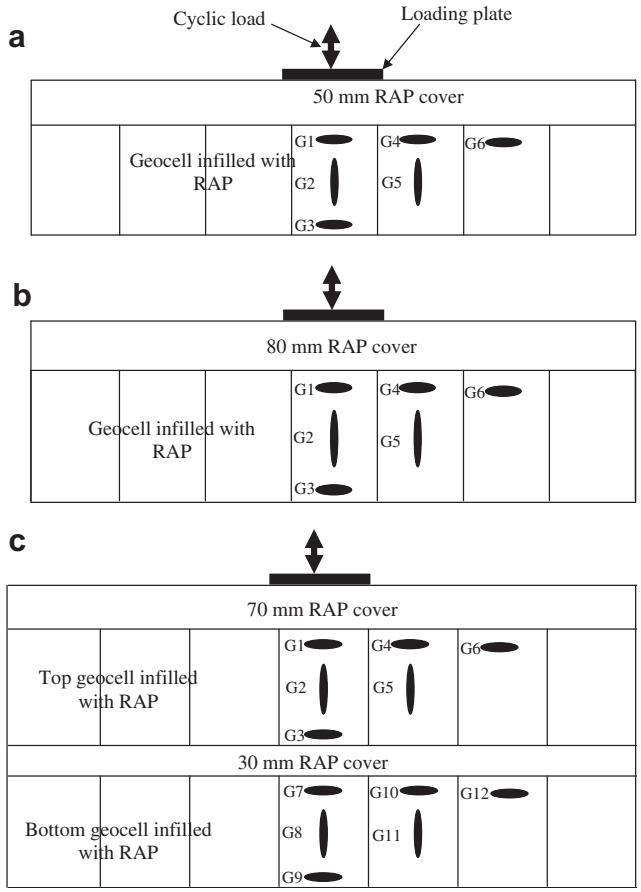

Fig. 14. Symbols, locations, and orientations of strain gages. (a) 0.15 m thick reinforced section, (b) 0.23 m thick reinforced section, (c) 0.30 m thick reinforced section.

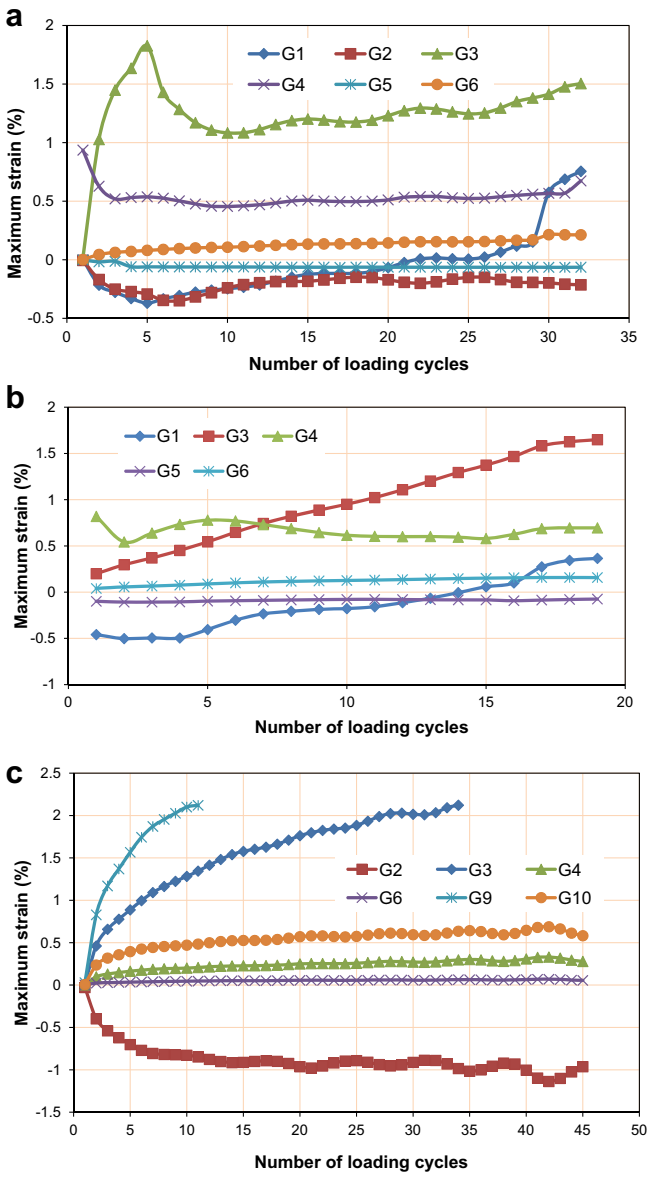

Fig. 15. Maximum strains on the geocell wall versus the number of loading cycles. (a) 0.15 m thick reinforced section, (b) 0.23 m thick reinforced section, (c) 0.30 m thick reinforced section.

For the unreinforced section, however, the stress distribution angle continued to decrease until failure, which demonstrated the unstable response behavior. The minimum stress distribution angles for the 0.15 m, 0.23 m, and 0.30 m thick reinforced and 0.30 m thick unreinforced bases were 20.5°, 22.0°, 25.5° and 18.5°, respectively. The stress distribution angle for the 0.30 m thick unreinforced base section could continue decreasing if the test had continued. Similar observations for the stress distribution angles were made by Han et al. (2011) for 0.25 m thick fractionated RAP bases (i.e. 33–36° for the reinforced bases and 26° for the unreinforced base) during full-scale moving wheel load tests. It can be concluded that the geocell reinforcement reduced the vertical stress by distributing the load to a wider area.

3.6. Strain in the geocell

Half-square grid general purpose strain gages were installed on the geocell walls to measure induced strains due to the deformation of the geocell under the application of the load. The surface of the geocell wall was smoothened by a sand paper and cleaned by isopropyl alcohol before installing the strain gages. The strain gages were then installed to the smoothened wall surface using Cyanoacrylate adhesive and then covered with N-1 (VH10L) general purpose coating material. Three strain gages were installed on the central cell just under the loading plate (one each at top, middle and bottom of the wall), two gages were installed at the top and middle of the geocell wall on the adjacent cell, and one gage was installed at the top of the geocell wall on the next neighboring cell as shown in Fig. 14, in which the symbol, location, and orientation of each strain gage are provided. The strain gages had grid resistance of 120 ± 0.6% ohms, gage factor of 2.1 ± 0.5%, grid length of 6.35 mm, and grid width of 3.18 mm. Since there were only six channels available in the data recorder for strain gages, only six strain gages (G2, G3, G4, G6, G9, and G10) were connected to the data recorder during the cyclic testing for the 0.30 m thick reinforced section and only the final readings were taken for the remaining six strain gages after the test. Strain gages affixed on the top and bottom of the geocell walls (G1, G3, G4, G6, G7, G9, G10, and G12) measured the horizontal strains while the strain gages affixed in the middle of the walls (G2, G5, G8, and G11) measured the vertical strains. The maximum strains induced at different locations of the geocell walls versus the number of loading cycles for the 0.15 m, 0.23 m, and 0.30 m thick reinforced sections are shown in Fig. 15. Positive and negative strains refer to tensile and compressive strains respectively. During the preparation of base courses, the middle strain gage on the central cell (G2) in the 0.23 m thick reinforced section and the top gages affixed on the central geocell of both top and bottom layers (G1 and G7) in the 0.30 m thick reinforced section were damaged; therefore, no strain was measured.

All the strain gages affixed to the bottom of the geocell wall showed horizontal tensile strains, among which G3 and G9 measured the highest values. The top gages affixed on the central geocell (G1) in the 0.15 m and 0.23 m thick reinforced sections first measured small horizontal compressive strains (i.e., slab behavior at a smaller deformation) and then horizontal tensile strains (i.e., tensioned membrane behavior at a larger deformation). G4 and G6 measured horizontal tensile strains with the least value on G6. All the middle gages (G2, G5, G8, and G11) showed vertical compressive strains irrespective of the locations of cells with the higher value on the central geocell. The final strains measured at the end of the test on the 0.30 m thick reinforced section were −0.4%, −1.3%, −1.2%, and 0.1% for G5, G8, G11, and G12 respectively. It should be pointed out that the data recorder could only record strains of up to 2%. Therefore, the two strain gauges in the 0.30 m thick reinforced section as shown in Fig. 15 reached this limit. From these measured strains, it can be concluded that the thickest geocell-reinforced base (0.30 m thick RAP base) behaved as a slab with bending resistance whereas the other two reinforced bases (0.15 m and 0.23 m thick RAP bases) showed such behavior for initial few loading cycles and then turned to tensioned membrane behavior when the deformation became larger.

4. Conclusions

This paper presents an experimental study to evaluate the performance of novel polymeric alloy (NPA) geocell-reinforced recycled asphalt pavement (RAP) bases over weak subgrade under cyclic loading. This study was conducted based on typical conditions in field for the construction of geocell-reinforced unpaved roads over weak subgrade. A nonwoven geotextile was placed between the subgrade and the geocell-reinforced RAP

base. The thickness of the RAP cover over the geocell was 50–80 mm and the thickness of the RAP between two layers of geocell was 30 mm. Three large-scale cyclic plate loading tests were conducted on geocell-reinforced RAP bases with thicknesses of 0.15, 0.23, and 0.30 m over a weak subgrade with a CBR value of approximately 2%. For a comparison purpose, a large-scale cyclic plate loading test was also conducted on an unreinforced RAP base. The following conclusions can be made from this study:

1) 100% recycled asphalt pavement (RAP) can be used as a base course material with geocell confinement as a sustainable roadway construction technology.
2) The geocell improved the performance of RAP bases over weak subgrade as compared with the unreinforced base section. The numbers of loading cycles at the 75 mm permanent deformation for the 0.15, 0.23, and 0.30 m thick reinforced RAP base sections were 6.4, 3.6, and 19.4 times that for the 0.30 m thick unreinforced RAP base section, respectively.
3) Based on the shakedown theory, the geocell-reinforced RAP bases showed a stable response whereas the unreinforced RAP base showed an unstable response.
4) The geocell significantly increased the percentage of resilient deformation of the RAP base.
5) The geocell reinforcement reduced the vertical stresses transferred to the subgrade by distributing the load over a wider area.
6) The measured vertical stresses in the unreinforced section increased with the number of load cycles until failure, whereas those in the reinforced sections increased in the first few cycles and then decreased or became constant due to the slab or tensioned membrane effect of the geocell-reinforced layer.
7) The strain measurements showed that the thicker geocell-reinforced RAP base behaved as a slab with bending resistance and the thinner base behaved as a slab initially at a smaller deformation and then as a tensioned membrane at a larger deformation.
8) The infill density influenced the performance of the geocell-reinforced RAP base section.

Acknowledgments

This research was sponsored by the Mid-America Transportation Research Center. The geocell material used in this research was provided by PRS Mediterranean, Ltd. in Israel. RAP materials were supplied by R.D. Johnson Excavating, Co. Mr. Howard Jim Weaver, the laboratory manager, Mr. Kahle Loveless and Mr. Aj Rahman, undergraduate students, in the Department of Civil, Environmental, and Architectural Engineering (CEAE) at the University of Kansas (KU) provided great assistance during the laboratory tests. The authors appreciate all the above support.

References

American Society for Testing and Materials (ASTM C1252-06). Standard Test Methods for Uncompacted Void Content of Fine Aggregate (as Influenced by Particle Shape, Surface Texture, and Grading).
American Society for Testing and Materials (ASTM C127-07). Standard Test Method for Density, Relative Density (Specific Gravity), and Absorption of Coarse Aggregate.
American Society for Testing and Materials (ASTM C128-07a). Standard Test Method for Density, Relative Density (Specific Gravity), and Absorption of Fine Aggregate.
American Society for Testing and Materials (ASTM D1556-07). Standard Test Method for Density and Unit Weight of Soil in Place by the Sand-Cone Method.
American Society for Testing and Materials (ASTM D1856-09). Standard Test Method for Recovery of Asphalt from Solution by Abson Method.
American Society for Testing and Materials (ASTM D2172/D2172M-11). Standard Test Methods for Quantitative Extraction of Bitumen from Bituminous Paving Mixtures.
American Society for Testing and Materials (ASTM D4318-10). Standard Test Methods for Liquid Limit, Plastic Limit, and Plasticity index of soils.
American Society for Testing and Materials (ASTM D6307-10). Standard Test Method for Asphalt Content of Hot-Mix Asphalt by Ignition Method.
Bennert, T., Maher, A., 2005. The Development of a Performance Specification for Granular Base and Subbase Material, Report No. FHWA-NJ-2005-003, p. 55.
Boushehrian, A.H., Hataf, N., Ghahramani, A., 2011. Modeling of the cyclic behavior of shallow foundations resting on geomesh and grid-anchor reinforced sand. Geotextiles and Geomembranes 29 (3), 242–248.
Canadian Strategic Highway Research Program, 2000. Asphalt: Current Issues and Research Needs. Millennium Research Brief No.1, 6 p.
Giroud, J.P., Han, J., 2004a. Design method for geogrid-reinforced unpaved roads. I. development of design method. Journal of Geotechnical and Geoenvironmental Engineering, ASCE 130 (8), 775–786.
Giroud, J.P., Han, J., 2004b. Design method for geogrid-reinforced unpaved roads. II. calibration of applications. Journal of Geotechnical and Geoenvironmental Engineering, ASCE 130 (8), 787–797.
Hammitt, G.M., 1974. Thickness Requirement for Unsurfaced Roads and Airfields, Bare Base Support. The U.S. Army Engineer Waterways Experiment Station, CE, Vicksburg, Miss. Project 3782-65, Technical Rep. S-70-5.
Han, J., Pokharel, S.K., Yang, X., Manandhar, C., Leshchinsky, D., Halahmi, I., Parsons, R.L., 2011. Performance of geocell-reinforced RAP bases over weak subgrade under full-scale moving wheel loads. ASCE Journal of Materials in Civil Engineering 23 (11), 1525–1534.
Han, J., Yang, X.M., Leshchinsky, D., Parsons, R.L., 2008. Behavior of geocell-reinforced sand under a vertical load. Journal of Transportation Research Board 2045, 95–101.
Holtz, R.D., Christopher, B.R., Berg, R.B., 2008. Geosynthetic Design and Construction Guidelines. National Institute of Highway. Publication No. FHWA NHI-07–092, 612 p.
Latha, G.M., Murthy, V.S., 2007. Effects of reinforcement form on the behavior of geosynthetic reinforced sand. Geotextiles and Geomembranes 25 (1), 23–32.
Locander, R., 2009. Analysis of using Reclaimed Asphalt Pavement (RAP) as a Base Course Material. Colorado Department of Transportation DTD Applied Research and Innovation Branch. Report No. CDOT-2009-5, 61 p.
McGarrah, E.J., 2007. Evaluation of Current Practices of Reclaimed Asphalt Pavement/Virgin Aggregate as Base Course Material. Washington State Department of Transportation. Research report, 41 p.
Moghaddas Tafreshi, S.N., Dawson, A.R., 2010a. Comparison of bearing capacity of a strip footing supported on sand reinforced with 3D and with planar geotextile. Geotextiles and Geomembranes 28 (1), 72–84.
Moghaddas Tafreshi, S.N., Dawson, A.R., 2010b. Behaviour of footings on reinforced sand subjected to repeated loading - Comparing use of 3D and planar geotextile. Geotextiles and Geomembranes 28 (5), 434–447.
Moghaddas Tafreshi, S.N., Dawson, A.R., 2012. A comparison of static and cyclic loading responses of foundations on geocell-reinforced sand. Geotextiles and Geomembranes 32 (3), 55–68.
Muki, R., 1961. Asymmetric Problems of the Theory of Elasticity for a Semi-infinite Solid and a Thick Plate. In: Progress in Solid Mechanics, vol. 1. North-Holland Publishing Co., Amsterdam.
Pokharel, S.K., 2010. Experimental Study on Geocell-Reinforced Bases under Static and Dynamic Loadings. Ph.D. dissertation, CEAE Department, the University of Kansas.
Pokharel, S., Han, J., Leshchinsky, D., Parsons, R.L., Halahmi, I., 2010. Investigation of factors influencing behavior of single geocell-reinforced bases under static loading. Geotextiles and Geomembranes 28 (6), 570–578.
Pokharel, S.K., Han, J., Manandhar, C., Yang, X.M., Leshchinsky, D., Halahmi, I., Parsons, R.L., 2011. Accelerated pavement testing of geocell-reinforced unpaved roads over weak subgrade. Journal of the Transportation Research Board 2204 (2), 67–75.
Qian, Y., Han, J., Pokharel, S.K., Parsons, R.L., 2011. Stress analysis on triangular aperture geogrid-reinforced bases over weak subgrade under cyclic loading – an experimental study. Journal of the Transportation Research Board 2204 (2), 83–91.
Qian, Y., Han, J., Pokharel, S.K., Parsons, R.L. Performance of triangular aperture geogrid-reinforced base courses over weak subgrade under cyclic loading. ASCE Journal of Materials in Civil Engineering, submitted for publication.
Rajagopal, K., Krishnaswamy, N.R., Latha, G.M., 1999. Behaviour of sand confined with single and multiple geocells. Geotextiles and Geomembranes 17 (3), 171–184.
Taha, R., Ali, G., Basma, A., Al-Turk, O., 1999. Evaluation of reclaimed asphalt pavement aggregate in road bases and subbases. Journal of Transportation Research Board 1652 (1), 264–269.
Thakur, J.K., Han, J., Leshchinky, D., Halahmi, I., Parsons, R.L., 2011. Creep deformation of unreinforced and geocell-reinforced recycled asphalt pavements. In: Han, J., Alzamora, D.E. (Eds.), Advances in Geotechnical Engineering, Geotechnical Special Publication No. 211, Proceedings of GeoFrontiers 2011, pp. 4723–4732. Dallas, TX, March 13 to 16, 2011.
Thakur, J.K., Han, J., Pokharel, S.K., Parsons, R.L., 2012. A large test box study on geocell-reinforced recycled asphalt pavement (RAP) bases over weak subgrade under cyclic loading. In: Hryciw, R.D., Athanasopoulos-Zekkos, A., Yesiller, N.

(Eds.), GeoCongress 2012, Oakland, California, USA, March 25–29, State of the Art and Practice in Geotechnical Engineering, Geotechnical Special Publication No. 225, pp. 1562–1571.

User Guidelines for Byproducts and Secondary Use Materials in Pavement Construction, 2008. Retrieved June 17, 2010 from: http://www.rmrc.unh.edu/tools/uguidelines/rap134.asp.

Webster, S.L., Brown, R.W., Porter, J.R., 1994. Force Projection Site Evaluation Using the Electric Cone Penetrometer (ECP) and the Dynamic Cone Penetrometer (DCP). U.S. Army Corps of Engineers, Washington, D.C., Technical Report GL-94-17, p. 172.

Yang, X., Han, J., Pokharel, S.K., Manandhar, C., Parsons, R.L., Leshchinsky, D., Halahmi, I., 2012. Accelerated pavement testing of unpaved roads with geocell-reinforced sand bases. Geotextiles and Geomembranes 32, 95–103.

Yuu, J., Han, J., Rosen, A., Parsons, R.L., Leshchinsky, D., 2008. Technical review of geocell-reinforced base courses over weak subgrade. In: Proceedings of the First Pan American Geosynthetics Conference & Exhibition, Cancún, Mexico, 2–5 March 2008, pp. 1022–1030.

Zhang, L., Zhao, M., Zou, X., Zhao, H., 2009. Deformation analysis of geocell reinforcement using Winkler model. Geotextiles and Geomembranes 36, 977–983.

Nomenclature

α: the stress distribution angle in degree with respect to the vertical
CBR: California Bearing Ratio (%)
C_u: vane shear strength of subgrade (kPa)
h: the thickness of the base course (m)
P: the applied load (kN)
PI: Penetration Index (mm/blow)
p_i: the distributed vertical stress at the center of the interface of base course and subgrade (kPa)
r: the radius of the tire contact area (m)